22nd International Congress of Mechanical Engineering (COBEM 2013)
November 3-7, 2013, Ribeirão Preto, SP, Brazil

TOPOLOGICAL REMESHING AND LOCALLY SUPPORTED SMOOTHING FOR BUBBLE COALESCENCE IN TWO-PHASE FLOWS

Gustavo Charles P. de Oliveira, tavolesliv@gmail.com
Norberto Mangiavacchi, norberto@uerj.br
State University of Rio de Janeiro, Faculty of Engineering, Rio de Janeiro, RJ, Brazil, 20940-903

Gustavo Anjos, rabello@mit.edu
Massachusetts Institute of Technology, Department of Nuclear Science and Engineering, Cambridge, USA, MA 02139

John R. Thome, john.thome@epfl.ch
École Polytechnique Fédéral de Lausanne, LTCM - Laboratoire de Transfert de Chaleur et de Masse, Station 9, Lausanne, Switzerland, CH-1015

Abstract. *A dual strategy of remeshing and smoothing operations is introduced. At the forefront, the Arbitrary Lagrangian-Eulerian/Finite Element (ALE/FE) approach is introduced not only to discretize the continuum filled by the liquid and vapor phases but only to represent their common interface by computational elements. In synchrony, a Level-Set (LS) methodology accompanies the former by determining coalescing regions. This work presents a two-dimensional idealized model concerning the numerical modeling of the coalescence between two circular bubbles immersed in stagnant liquid. While the ALE/FE approach can guarantee suitable remeshing to recover the structure of the mesh modifications changeed after the thin liquid film disruption, the LS strategy locally determines the coalescing region by handling a function of compact support. The effect of the collapse is assuaged and any sharpnesses owing to local topological changes occurring in the contact region tend to be less protruding by smoothing. Two-dimensional numerical results show that this incipient methodology is promising in regard to coalescence studies and is able to be extended, a posteriori, to three-dimensional cases. Mainly headed to treat bubble interactions, these strategies aim to be embodied, in the sequel, into a two-phase flow context, especially to simulate the coalescence taking place in transitional regions of passage from bubbly-to-slug and slug-to-annular patterns.*

Keywords: *Bubble coalescence, ALE formulation, Level-Set, Finite Element, Two-Phase Flow.*

1. INTRODUCTION

In view of the growing field of applications involving multiphase flows, numerical tools have been developed to provide supplemmentary comprehension about the complex dynamics ocurring at interfacial regions shared by different fluids in their different phases. Inserted into this wider scope, gas-liquid flows cover a considerable range. They are present in chemical plants, oil pipelines, microevaporators, heat exchangers, cooling systems, just to cite a few examples. Some important patterns of two-phase flows are distinguished when gas bubbles permeate a continuum region of liquid either in a dispersive and disordered way, such as *bubbly* flows, or as elongated bubbles separated by liquid gaps, such as *slug* flows. Depending on the flow, the bubbles' surfaces may undergo plentiful transformations concerning their topology while interacting with one another. Generally, coalescence phenomena are initiated from these settings and their numerical simulation have been under potential interest of the MCFD (Multiphase Computational Fluid Dynamics).

Recent papers evince the bubble coalescence as a relevant issue. For instance, Consolini and Thome (2010) included the coalescence in their analysis of the thin evaporating film present in micro-channel slug flows by verifying how it may influence the heat transfer. Coalescence was included by Ekambara *et al.* (2012) in their numerical modeling of gas-liquid bubbly flows. Coulibaly *et al.* (2013) studied the bubble coalescence in subcooled nucleate pool boiling cases. On the other hand, efficient MCFD models to represent the coalescence are on the summit of discussions. This work aims to introduce a developing approach to assuage severe topological changes caused by the coalescence between two bubbles based on a combination between an ALE (Arbitrary Lagrangian-Eulerian) moving mesh formulation coupled with the Finite Element method and a Level-Set strategy enriched with a function whose support determines the coalescing region. Henceforward, we will refer to these strategies by the acronyms ALE/FE and LS.

Some strands of moving mesh methods applied to two-phase flows were lately disseminated in the literature as ALE/FE by dos Anjos (2012), PFEM (Particle Finite Element) by Mier-Torrecilla *et al.* (2011), and MMIT (Moving-Mesh Interface Tracking) by Quan (2011), Quan *et al.* (2009), Quan and Schmidt (2007). In all of them, the interface is described by computational elements (nodes, edges, faces) upon a body-fitted Lagrangian fashion. Consequently, the nodes, primarily, are advected with the own flow velocity, so that the condition of sharp interface (zero-thickness) is kept longer.

This capability shows a powerful advantage to simulate coalescence since the bubbles' boundaries deform as material surfaces. In the vein of these Lagrangian-like methods, another approach including LS imprints was presented by Sousa and Mangiavacchi (2005) at which the values of the level-set function is stored in each mesh node being, therefore, exempted of further calculations to attain smoothness. This work is rooted in a similar basis as regards the LS methodology, but it handles geometrical operations to remedy the mass unbalance that might come to pass at the coalescence region instead having to perform calculations of smoothing functions. The method also has the advantage to capture topological complexities occurring in the liquid thin film region between the bubbles because an algorithm based on distance calculations is applied. Next, the coalescence region is numerically determined by a function that pervades the original level-set function to confine the elements closer to the interfaces within a tolerance domain in order to mimic the real physics. This forcibly narrowed region is referred as *combination zone*.

Although the ALE/FE be the mechanism used for discretization of both computational domain and interfaces, the LS strategy is appended as a tool to determine the combination zone where the coalescence should take place. Examples of LS methods coupled to FE are Groß *et al.* (2006), in the context of multiphase flows, and Li and Shoppie (2011), concerning the interface-fitted representation. Aside, a general overview about LS methods is conducted by Osher and Fedkiw (2001).

Apart from their physical constitution, bubbles (also drops) may be recognized mathematically as topological surfaces - see Bloch (1956). In real applications involving two-phase flows, their boundaries may assume varying shapes depending on the flow pattern at which they emerge. Owing to this topological richness, formal terminologies could be coined. Shape regimes of bubbles were previously presented by Clift *et al.* (1978) in two major classes: static (sessile, pendant and floating bubbles) and free-motion (spherical, ellipsoidal and "spherical-cap" bubbles). Notwithstanding, incremental terminology appeared in the current literature. Some examples are cited by Michaelides (2006), such as "spherical cap with closed wake", "oblate ellipsoidal disk", and "skirted with wavy unsteady skirt".

At this point, it is worth to remember a few adimensional numbers that are related to bubble dynamics. Some of them are used to determine the shape regimes aforementioned. For instance, when interfacial effects are not negligible in the flow, the Weber number, *We*, is used to quantify the ratio between inertia and surface tension forces, whereas the Eötvös number, *Eo*, is used to quantify the ratio between buoyancy and surface tension forces. Besides, the classical Reynolds and Froude numbers, *Re* and *Fr*, are used in two-phase correlations as well. Equation (1) groups the definition of these numbers.

$$We = \frac{\rho_0 L0 U0^2}{\sigma_0}, \qquad Eo = \frac{\rho_0 g_0 D_0^2}{\sigma_0}, \qquad Re = \frac{U_0 L_0}{\nu_0}, \qquad Fr = \frac{U_0}{\sqrt{g_0 L_0}}, \tag{1}$$

where all the variables described are measures of reference chosen accordingly to the problem to be tackled, namely, lenght (L_0), velocity (U_0), density (ρ_0), gravity (g_0), diameter (D_0), surface tension (σ_0), and kinematic viscosity (ν_0). Furthermore, Eq. (2) defines another adimensional used to characterize the shape of bubbles. The Morton number *Mo* is originated by combining powers of We, Fr, and Re.

$$Mo = \frac{We^3}{FrRe^4} \tag{2}$$

Some two-phase flow patterns are characterized by bubble interactions and are being extensively studied. We can refer to Cheng *et al.* (2008) for a review of flow patterns and maps. Consequently, coalescence phenomena observed in these flows are motivating a growing research interest. Recently, bubble dynamics studies viewing mass transfer purposes, for instance, were conducted by Agrawal (2013). Regarding to nucleate boiling and chemical process, we can cite Jingliang *et al.* (2012).

Other patterns showing profuse topological changes are also identified in nuclear reactor applications as depicted at Fig. 1, an abridged picture extracted from Shen *et al.* (2012) which shows gas-liquid structures appearing on upward flows in a narrow rectangular channel. In such patterns, bubble coalescence is propitious to happen mainly amid regime transitions and this issue is addressed by Julia and Hibiki (2011).

In horizontal microchannel two-phase flows, regime transitions are also observed. Among them, the bubble-to-slug is a particular regime we look on. Figures 2 and 3 show macro-to-microchannel transition curves obtained through experimental studies in two-phase flows performed by Ong and Thome (2011) for the artificial refrigerant fluids R236fa and R134a, respectively. Therein, it is explicit the zone where the coalescing bubble pattern takes place. They declare that, in some cases, the bubbles violently coalesce and no clear interface between the two phases can be seen. It is also emphasized in Revellin *et al.* (2008) that collision of bubbles in microchannels may be one of the most important parameters influencing flow pattern transition. In turn, such topological changes may render a difficult task when computationally tackled through MCFD methods.

Before the profuse topological complexity observed experimentally in several gas-liquid two-phase flow patterns, one seeks MCFD methods more and more effective to compensate shortcomings produced by discretization processes. Mass conservation errors, which account for a bad representation of the physical problem, could be emphasized as an example.

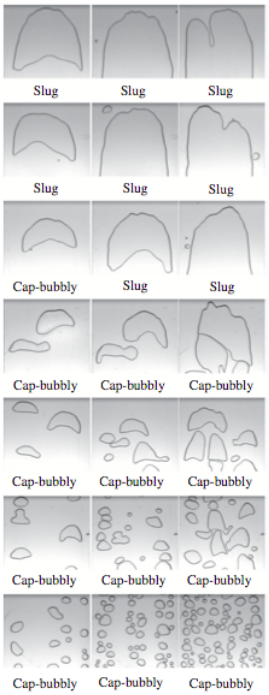

Figure 1: Two-phase upward flow structures in a narrow rectangular channel. Adapted from Shen *et al.* (2012).

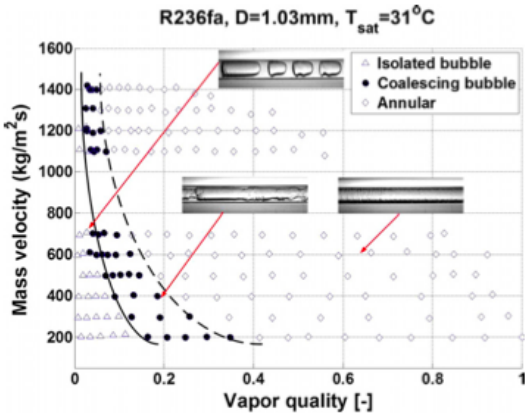

Figure 2: Flow pattern transition lines for R236fa. Extracted from Ong and Thome (2011).

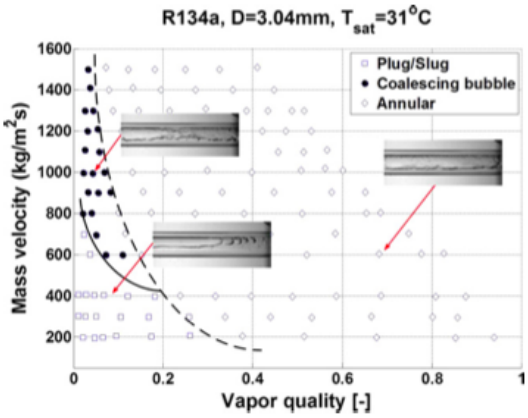

Figure 3: Flow pattern transition lines for R134a. Extracted from Ong and Thome (2011).

It is our interest in this work to emphasize how promising the ALE/FE approach may be to resolve computationally bubble coalescence phenomena. Certainly, one of its most powerful characteristics is treating both liquid and gas phases with the same computational mesh. This is a positive point as regards tracking the interfacial dynamics.

This paper is organized as follows: Sec. 2. introduces the equations governing the two-phase fluid flow system and explains the scheme used to calculate important properties such as curvature; Sec. 3.describes an algorithm based on the ALE/FE coupled to LS approch to face the coalescence problem as well as the overall methodology. We consider a bidimensional simplified model of head-on coalescence between two circular bubbles with analogous extension to three-dimensional cases; in the Sec. 4. some numerical results are showed and followed by discussions, and Sec. 5 ends up the paper with some conclusions.

2. GOVERNING EQUATIONS

The governing equations used in this work take an ALE frame into account in their formulation. Some arbitrariness is given to the mesh nodes move freely when the ALE description is used. Alternatively, the nodes either may keep stopped as an Eulerian fashion, or move together with the fluid, or even walk to a specified direction. This freedom permits a continued rezoning capability. Additionally, larger distortions are handled with good resolution. Thus, the acme of the ALE approach is achieved.

To reach its proposal, the ALE methodology establishes an "intermediary" domain called *referential domain* to make an interplay between the material and spacial domains used to map the movement. Under a mathematical language, the ALE description can be understood through homeomorphisms. According to Donea *et al.* (2004), from these latter mappings, the velocity field is thereby called *convective velocity* and written as

$$\boldsymbol{c} = \boldsymbol{v} - \hat{\boldsymbol{v}}, \tag{3}$$

where $\boldsymbol{v}$ is the *fluid velocity* and $\hat{\boldsymbol{v}}$ is the *mesh velocity*.

For the two-phase modeling discussed here, we consider that the fluid properties are constant everywhere inside the liquid and vapor phases, differing by a discontinuity jump only over the interface locus. In other words, we use a separated flow model that leads to a simplified version of the momentum equation (see, for instance, Hewitt and Hall-Taylor (1970)). Furthermore, the incompressibility condition is assumed to be valid for both phases. Gravitational and interfacial forces are considered to be present in the model as well. By using $\boldsymbol{c}$, all these hypotheses lead to the following pair of adimensional equations valid for each phase separatedly.

$$\frac{\partial \boldsymbol{v}}{\partial t} + \boldsymbol{c} \cdot \nabla \boldsymbol{v} = -\frac{1}{\rho}\nabla p + \frac{1}{Re}\nabla \cdot \left[\nu \left(\nabla \boldsymbol{v} + \nabla \boldsymbol{v}^{T}\right)\right] + \frac{1}{Fr^2}\boldsymbol{g} + \frac{1}{We}\boldsymbol{f} \tag{4}$$

$$\nabla \cdot \boldsymbol{v} = 0, \tag{5}$$

where $\boldsymbol{v}$ is the fluid velocity, p the pressure, ρ the density, ν the kinematic viscosity, $\boldsymbol{g}$ the gravitational force. Fr and We have already been defined in the Eq. (1). $\boldsymbol{f}$ accounts for interfacial effects and is given by

$$\boldsymbol{f} = \sigma\kappa\boldsymbol{n}, \tag{6}$$

where σ is the surface tension, κ the curvature locally evaluated over the interface, and $\boldsymbol{n}$ the unit normal vector over each interface node pointing outward the vapor phase. The discrete process to calculate the unit normal vector in two-dimensional domains takes two properties into account. Firstly, the interface is a closed curve represented by a set of linear elements and, hence, structured. That is to say, each interface node has always two neighbor elements. Secondly, the normal vectors for each neighbor element can be obtained by orthogonalizing the unit tangent vectors to each element, which, in fact, are obtained by normalizing the element length itself. In turn, the normal vector for the shared node is evaluated by summing the contributions of the normal elemental vectors. This scheme is depicted in the Fig. 4. Mathematically, if $\boldsymbol{n}(e_{L,i}), \boldsymbol{n}(e_{R,i})$ are the unit normal vectors evaluated over the neighbor elements respectively at left and at right of the interface node $\boldsymbol{x}_i$, then,

$$\boldsymbol{n}(e_{L,i}) = \boldsymbol{R}_{\pi/2}\left[\boldsymbol{t}(e_{L,i})\right], \quad \boldsymbol{n}(e_{R,i}) = \boldsymbol{R}_{\pi/2}\left[\boldsymbol{t}(e_{R,i})\right], \tag{7}$$

where

$$\boldsymbol{t}(e_{L,i}) = \frac{\boldsymbol{x}_{L,i} - \boldsymbol{x}_i}{||\boldsymbol{x}_{L,i} - \boldsymbol{x}_i||}, \quad \boldsymbol{t}(e_{R,i}) = \frac{\boldsymbol{x}_{R,i} - \boldsymbol{x}_i}{||\boldsymbol{x}_{R,i} - \boldsymbol{x}_i||}. \tag{8}$$

Above, $\boldsymbol{x}_{L,i}, \boldsymbol{x}_{R,i}$ are the vertices of the neighbor elements not matching the interface node and $\boldsymbol{t}(e_{L,i}), \boldsymbol{t}(e_{R,i})$ their respective unit tangent vectors generated by the rotation matrix $\boldsymbol{R}_{\pi/2}$. Directly from Eqs. 7 and 8, we get

$$\boldsymbol{n}(\boldsymbol{x}_i) = \boldsymbol{n}(e_{L,i}) + \boldsymbol{n}(e_{R,i}) = \boldsymbol{R}_{\pi/2}\left[\boldsymbol{t}(e_{L,i}) + \boldsymbol{t}(e_{R,i})\right]. \tag{9}$$

Meanwhile, the curvature $\kappa(\boldsymbol{x}_i)$ is evaluated for each interface node by an approximation adapted from a formulae set of

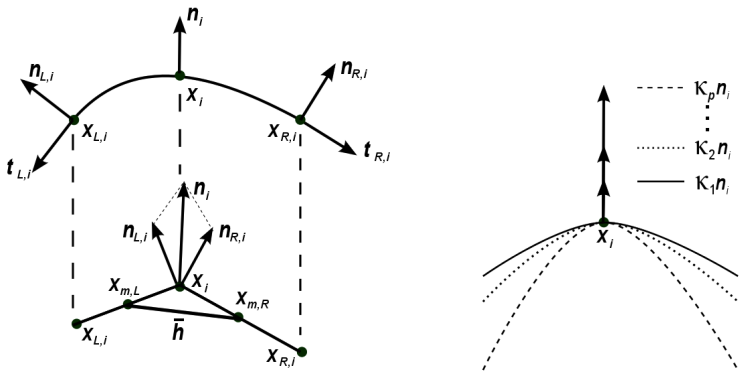

(a) (b)

Figure 4: Scheme for the calculation of the curvature: (a) continuous and discrete versions; (b) effect of the curvature upon the normal vector at $\boldsymbol{x}_i$.

the Frenet's frame, or, even more formally, *Frenet-Serret Theorem* - see Bloch (1956) - for curvature and torsion. Equation 10 is the continuous version of one among the Frenet's formulae relating κ and the unit vector tangent $\boldsymbol{t}$ to the interface.

$$\kappa \boldsymbol{n} = \frac{\partial \boldsymbol{t}}{\partial s} \approx \frac{\boldsymbol{t}(e_{L,i}) - \boldsymbol{t}(e_{R,i})}{\bar{h}}. \tag{10}$$

Since the elements $e_{L,i}, e_{R,i}$ do not have necessarily the same size, the evaluation of $\kappa(\boldsymbol{x}_i)$ is undertaken as an average distribution over the mean length $\bar{h}$ of the neighbor elements given by

$$\bar{h} = \frac{1}{2}(h_L + h_R), \tag{11}$$

where h_L, h_R are the lengths of the neighbor elements. Also depicted in Fig. 4, at left, it is seen that $\bar{h}$ binds the two centroidal points $\boldsymbol{x}_{m,L}, \boldsymbol{x}_{m,R}$. At right, a sketch was added only to illustrate how κ affects the normal vector $\boldsymbol{n}_i$ by stretching it. From Eq. 10, we infer that the higher the tangential derivative along the interface, the higher the norm of the vector $\kappa \boldsymbol{n}_i$, because if, for instance, we choose a sequence (κ_p) such that $\kappa_1 < \kappa_2 < \ldots < \kappa_p$, then

$$||\kappa_1 \boldsymbol{n}_i|| < ||\kappa_2 \boldsymbol{n}_i|| < \ldots < ||\kappa_p \boldsymbol{n}_i||. \tag{12}$$

In other words, high curvatures tend to magnify the normal vector at $\boldsymbol{x}_i$.

Additionally, the Heaviside function is used in this work to manage points near to interface sites. It identifies if an arbitrary node belongs to the liquid phase, the vapor phase, or the interface. Since its image is, in fact, the discrete set $\{0, 1\}$, it is not unexpected to assign a mean value to identify interface nodes and define H as

$$H(\boldsymbol{x}) := \begin{cases} 0, & \text{if } \boldsymbol{x} \equiv \boldsymbol{x}_L \\ 0.5, & \text{if } \boldsymbol{x} \equiv \boldsymbol{x}_I \\ 1, & \text{if } \boldsymbol{x} \equiv \boldsymbol{x}_V, \end{cases} \tag{13}$$

where the subscripts L, I, V stands for liquid, interface, and vapor.

Equation 6 is a version of the Continuum Surface Force (CSF) model introduced by Brackbill *et al.* (1992), in which the surface force was redesigned as a volumetric force. In terms of the aforementioned equations, the force $\boldsymbol{f}$ in the Eq. (6) is obtained by a FE procedure that solves the linear system given by

$$\frac{1}{We}\boldsymbol{M}\boldsymbol{f} = \frac{1}{We}\boldsymbol{\Sigma}\boldsymbol{G}H, \tag{14}$$

where $\boldsymbol{\Sigma}$ is a diagonal matrix whose entries are given by $\sigma\kappa_1, \sigma\kappa_2, \ldots, \sigma\kappa_P$, for P pressure nodes over the mesh. $\boldsymbol{G}$ is the gradient discrete matrix and H the Heaviside function.

3. METHODOLOGY: ALE/FE AND LEVEL-SET FOR BUBBLE COALESCENCE MODELING

In this section, we explain a combined methodology to simulate coalescing bubbles. On the one hand, the ALE/FE approach provides the main capability to remesh the thin film local region reconnecting computational elements affected by topological change. On the other hand, the LS strategy is focused on summing a function whose support is liable to determine the coalescing region. For simplicity, we start from an idealized two-dimensional model describing a "head-on" coalescence process between two rounded bubbles immersed in a liquid. Even though this model does not take the

deformation of the bubbles' surfaces into account, the idea behind it can be conveniently conveyed to three-dimensional problems with different bubble shapes because it is focused on the thin liquid film region and not strictly on any transient topology experienced by the surfaces.

First of all, it is convenient to use some definitions. Let $\Omega_{b,1}$ ($\Gamma_{b,1}$) and $\Omega_{b,2}$ ($\Gamma_{b,2}$) be the domains (boundaries) of the bubbles in vapor phase, and $\Omega_{f,\epsilon}$ the in-between region of liquid thin film near the bubbles. ϵ is a small parameter related to the minimum distance between $\Gamma_{b,1}$ and $\Gamma_{b,2}$. In this discussion, the bulk region of liquid far from the thin film region whose scale is much bigger than ϵ is left untreated. It is feasible to set extreme points $\bar{\boldsymbol{x}}_1, \bar{\boldsymbol{x}}_2$, where $\bar{\boldsymbol{x}}_1 \in \Gamma_{b,1}$ and $\bar{\boldsymbol{x}}_2 \in \Gamma_{b,2}$ to perform limits for the minimum distance between the bubbles. Figure 5 depicts the idealized two-dimensional model, whereas Fig. 6 is an augmented view of the continuous thin film region.

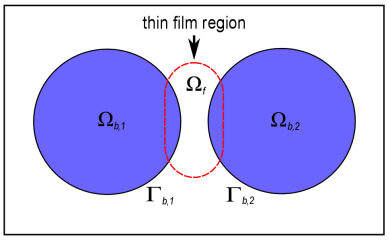

Figure 5: Two-dimensional idealized model for two near bubbles instantly before the head-on coalescence.

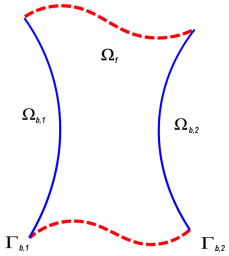

Figure 6: Augmented view of the liquid thin film region between two near bubbles.

In order to represent discretely the coalescence process through the ALE/FE approach, we will refer to Fig. 7, which is a sequential sketch showing the coalescence in three steps. For now, it is enough recognize the edges in black representing the part of the mesh defined as vapor phase; the edges in red, the liquid phase, and the edges in blue, the interfaces. As we have already noted at first glance, one of the main characteristics of the ALE/FE methodology is to describe the bubbles interfaces as nodes, edges, and faces. In this manner, the interfaces $\Gamma_{b,1}, \Gamma_{b,2}$ are made up by interconnected edges whose nodes are part of the same mesh used to discretize the liquid phase. For the sake of this sharing, the elements belonging to the thin film region can be tracked and identified as elements in coalescence so that they are, later, carried forward to vapor phase and marked as elements of this phase.

Yet with reference to the Fig. 7, the dashed green line represents the distance ϵ between the bubbles. In (a) the elements filled in red were intentionally marked as coalescing elements to work as target of the explanation. Since the elements are identified, geometrical operations (insertion, deletion, and flipping) are performed upon the nodes and edges in order to adapt the mesh, keep its quality and correct eventual mass unbalance. This step is represented in (b). The edges in yellow are inserted after the deletion operations that occurr to break up the interface and mediate the merging process. That is to say, the liquid is squeezed out while the thin film is undone and the onset of the coalescence starts off. In the sequel, (c) depicts the third step, when the coalescence process is evolving. At this stage, the yellow edges were replaced with black edges to highlight the merging process. As the simulation runs, similar transformations tend to be carried out by the code for the elements within the thin film region that obey the proximity criterion based on the minimum distance ϵ.

The minimum distance between the bubbles can be calculated by using the well-known $\mathbb{R}^n$ formula for distance between vectors

$$d(\boldsymbol{x}, \boldsymbol{y}) = \left[\sum_{i=1}^{n} (x_i - y_i)^2 \right]^{1/2} \tag{15}$$

if the arguments above are replaced with the extreme points $\bar{\boldsymbol{x}}_1$ and $\bar{\boldsymbol{x}}_2$. On the other hand, the minimum distance has to be determined by a numerical procedure which should span all the pairs of nodes belonging to $\Gamma_{b,1}$ and $\Gamma_{b,2}$, but inside a combination zone limited by another numerical artifice. Consequently, this combination zone tends to reduce calculations, since it is not necessary to go through all the interface nodes in order to find the minimum distance. In Quan *et al.* (2009), an algorithm based on the creation of a combination zone to simulate the head-on bubble coalescence is tested. However,

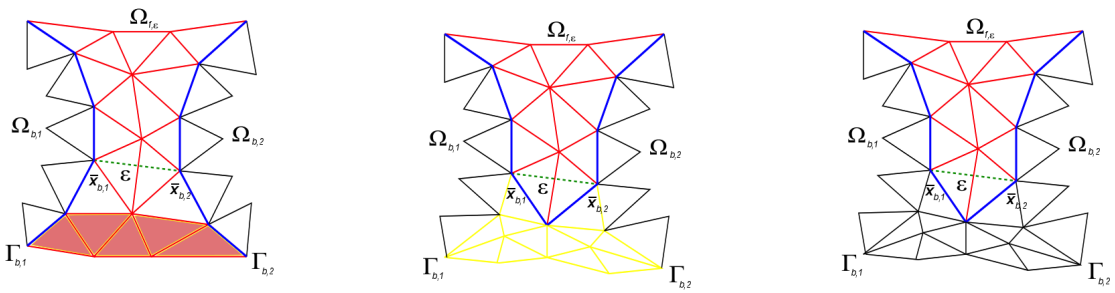

Figure 7: ALE/FE discretization of the thin film region between two bubbles: (a) before the coalescence; (b) onset of coalescence; (c) during the coalescence.

the author points out that not only the combination zone but also the process to determine it is a task depending on the problem and should be tuned for each case.

In seeking of the determination of the combination zone between the two bubbles, we invoke a LS context by defining particular functions. These functions, in the whole, not only specify the interface nodes, but also manage the local smoothing of the coalescing elements. Let ϕ be the standard level-set function defined as

$$\phi(\boldsymbol{x}) := \min_{\boldsymbol{x}_{I,k} \in \Gamma_{b,k}} \{d(\boldsymbol{x}, \boldsymbol{x}_{I,1}), d(\boldsymbol{x}, \boldsymbol{x}_{I,2})\}\,. \tag{16}$$

Since two interfaces are nearby each other, ϕ is introduced to detect the interface nodes belonging to the boundary of the bubbles and responding for the curve of contour zero. Before the coalescence, the bubbles are separated by a tiny distance. However, numerically, it is convenient to establish ϵ as the limiting parameter from which the coalescence should start off. Consequently, all the elements inside this delimited area will undergo geometrical transformations and will be pending for remeshing. In the new methodology now introduced, we wish that the coalescing elements are kept subordinate to a function W_ϵ whose support will affect directly the zero contour of the level-set function. In other words, W_ϵ pervades the combination zone to cause smoothness in the curve identified by $\phi(\boldsymbol{x}) = 0$. We call W_ϵ a *blending function*, which is defined as

$$W_\epsilon(\boldsymbol{x}) := \begin{cases} 1 - \dfrac{||\boldsymbol{x}||}{\epsilon}, & \text{if } \boldsymbol{x} \in \Omega_{f,\epsilon} \\ \\ 0, & \text{otherwise.} \end{cases} \tag{17}$$

Similarly to ϕ, W_ϵ also is cone-shaped, but centered in the combination zone and having a small support. When W_ϵ "pierces" ϕ so blending their contributions, a new function $\tilde{\phi}$ is created by defining

$$\tilde{\phi}(\boldsymbol{x}) := \phi(\boldsymbol{x}) - 2\epsilon W_\epsilon(\boldsymbol{x}). \tag{18}$$

Further details about $\tilde{\phi}(\boldsymbol{x})$ are given in the next section.

4. NUMERICAL RESULTS AND DISCUSSIONS

Some numerical tests are showed in this section. Figure 8 is a plot of $\tilde{\phi}$ for a two-dimensional domain of size $6D \times 4D$, where D is the diameter of the bubbles. The small coniform hill in the middle displays the contribution of W_ϵ. As a result, the contour zero of $\tilde{\phi}$ is a new curve intercepted by a central bulb-like neck which foreshadows a bridge for the coalescence. Figure 9 shows the shaded contour zero of $\tilde{\phi}$ as well as the resulting curve under a simple layout. Figure 10 shows a version of the numerical steps to be managed by the blending function before and after the coalescence by considering a symbolic Delaunay triangularized domain as a preview for better future implementation.

Additionally, we present a numerical simulation of a oscillating drop immersed in a stagnant liquid in order to show the capability of the ALE/FE to capture topological changes of surface. This is a benchmark test concerning code validation and was performed by dos Anjos (2012) under a three-dimensional version. The domain of simulation is a square with dimensions $8D \times 8D$, where D is the drop diameter. Initially, the drop is slightly symmetrically ellipsoidal in relation to the $x-$axis. Apart from gravity effects, the drop is weakly perturbed so oscillating with an induced frequency ω of

$$\omega = \left[\frac{(n^3 - n)\sigma}{(\rho_{in} + \rho_{out})r^3}\right]^{1/2} \tag{19}$$

and decay amplitude of

$$a(t) = a_0 e^{-t/\tau}. \tag{20}$$

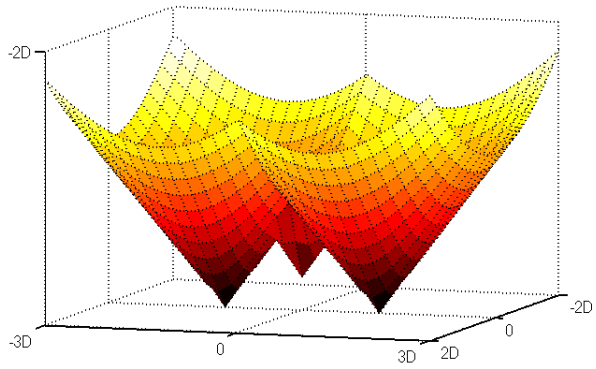

Figure 8: Function $\tilde{\phi}$ plotted over the coalescence domain $6D \times 4D$.

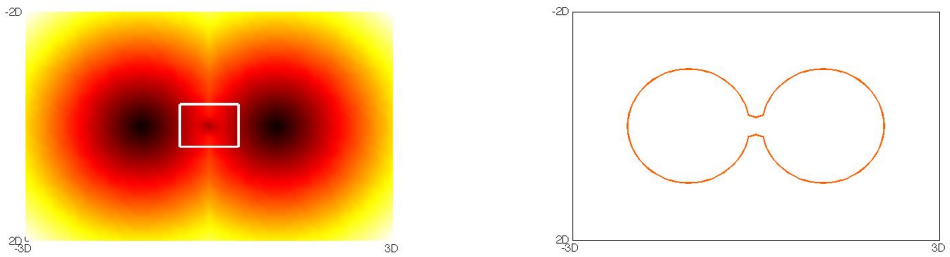

(a) (b)

Figure 9: Contour zero of $\tilde{\phi}$: (a) shaded, with the white rectangle highlighting the coalescing bridge; (b) simple curve.

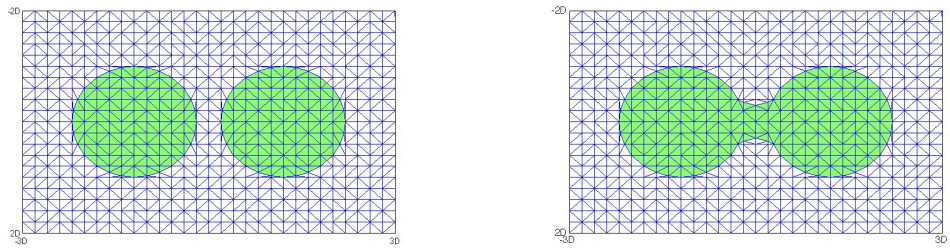

(a) (b)

Figure 10: Smoothing effect generated by the blending function: (a) before the coalescence; (b) after the coalescence.

In the Eqs. 19 and 20, n is the mode of perturbation, σ is the surface tension coefficient, ρ_{in}, ρ_{out} the densities of the internal and external fluids, r the drop radius, and ν the kinematic viscosity. When varying its diameter, the drop surface obeys the following time-depending equation

$$y(t) = y_0 + a(t)cos(\omega t), \tag{21}$$

where y_0 is the $y-$axis initial coordinate.

For the present simulation, all the parameters before mentioned were set as $n = 2$, $\sigma = 1$, $\rho_{in} = 1$, $\rho_{out} = 0.001$, $r = 0.5$, $\nu = 1$, $a_0 = 0.1r$, and $y_0 = 0$. Given the small external viscosity imposed, the oscillatory process is governed by interfacial forces and counterbalanced by convective forces. In the Fig. 11, it is depicted the image of the Heaviside function for the oscillating drop both in overview and augmented views. As it is seen, the interface region is notably distinguished by colors and higher refinement.

Five levels of adaptive refinement were applied over the interface mesh as exhibiting the accuracy of the method to accompany the topological changes of the interface. Figure 12 is a plot of the variation of amplitude *versus* time of the drop, i.e., it shows how the $y-$diameter oscillates along the time. Between the coarsest mesh, whose elements have a characteristic length of $h = 0.2$, and the finest mesh, with $h = 0.012$, three intermediary levels were simulated: $h = 0.1$, $h = 0.05$, and $h = 0.025$. In overall, the numerical solutions tend to the analytical solution and, consequently, better accuracy is achieved as the mesh is refined. Three particular plots of the mesh velocity field were extracted from the time interval $T = [0, 1.2]$ for a simulation with level $h = 0.025$, $CFL = 0.8$ and convenient time instants chosen inside T, namely, $t \approx 0.20\,s$; $t \approx 0.59\,s$, and $t \approx 0.71\,s$ are organized in the Fig. 13. Inside T, the drop completes a period

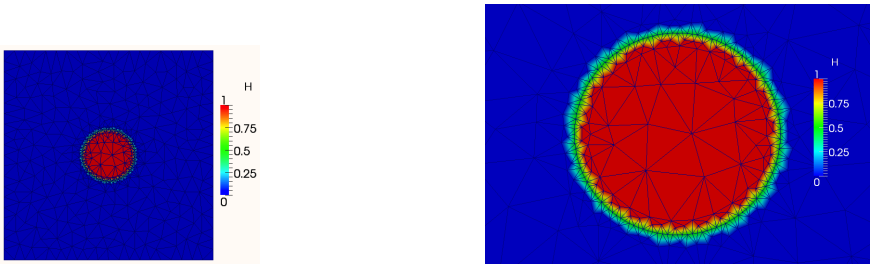

(a) (b)

Figure 11: Heaviside function detecting the interface region as well as the liquid and vapor phases for the oscillating drop test: (a) overview of the two-dimensional FE mesh; (b) FE mesh zoomed in.

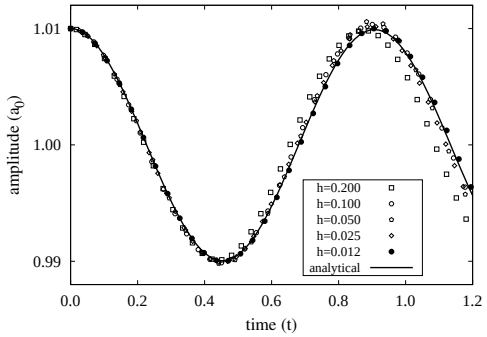

Figure 12: Comparative plot of the analytical diameter $y-$variation for the oscillating drop test against five increasing levels of interface local refinement.

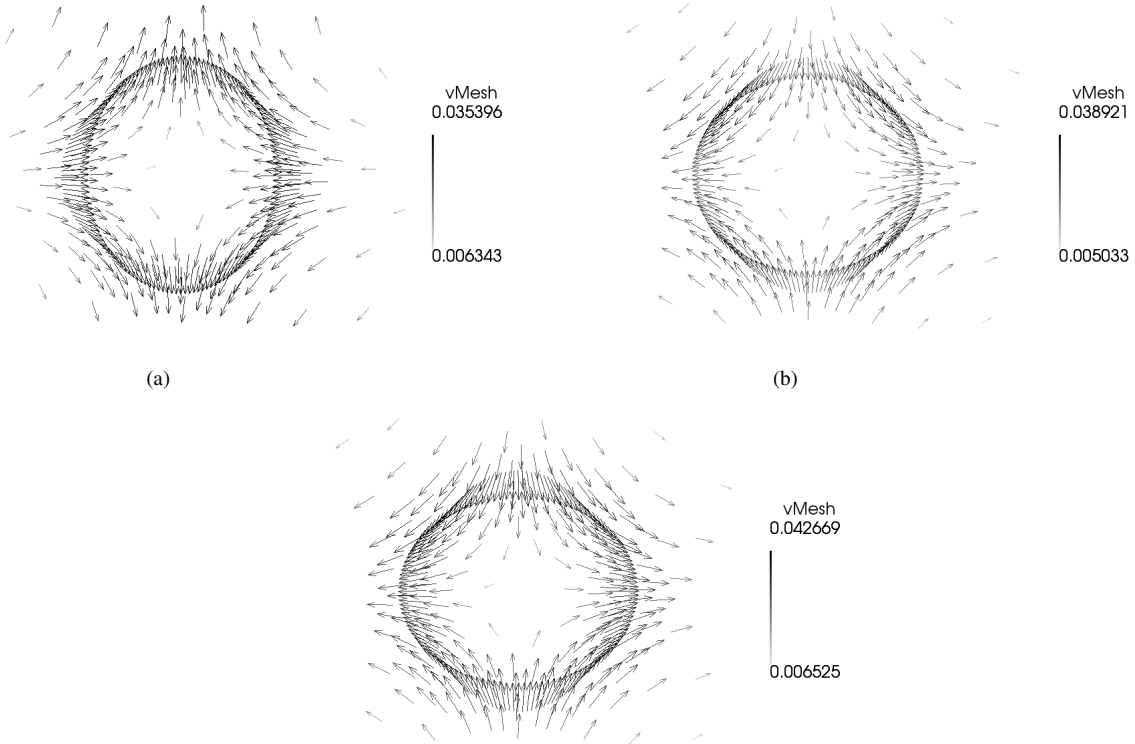

(a) (b)

(c)

Figure 13: Mesh velocity field surrounding the oscillating drop for three different times: (a) $t \approx 0.20\,s$; (b) $t \approx 0.59\,s$; (c) $t \approx 0.71\,s$.

of oscillation and the mesh velocity field changes accordingly as it can be observed. In (a), the drop begins to dilatate along the $y-$axis because of the perturbation imposed. Simultaneously, both the mesh points of the interface and those surrounding it are moved in order to follow the topological change of the surface and the external fluid layers pushed out. Inasmuch as the incompressibility constraint must to be satisfied, the drop is flattened in the $x-$axis. In (b), the drop is under inverse process and dilatates along the $x-$axis until achieving the sequential shape depicted in (c) after a few seconds. This process is repetitive along the periods of oscillation, other than by the direction of the vectors that is inverted after each peak of amplitude and does not require extensive analysis. Moreover, very small velocities are, indeed, expected to occur for the drop as it can be verified in each plot, where the magnitude of the mesh velocity field is scaled by the size of the vectors.

5. SUMMARY AND CONCLUSIONS

Purposes of this paper were: to address the bubble coalescence in two-phase flows with focus on a coupled approach between the ALE/FE and LS methodologies; to propose a numerical strategy to model the coalescence of two spherical bubbles by delimiting a combination zone that confines the liquid thin film region near the bubbles, and to present inceptive numerical results guided by the presented idea.

The standard level-set function was increased by a new blending function whose support determines locally the coalescing zone. Cumulatively, this cone-shaped function produces a smoothing effect upon the original level-set function which reflects over the curve of contour zero when forming a central bulb that induces the coalescence. Thereafter, the instantaneity of the real coalescence is condensated into a numerical step.

Additionally, a benchmark test based on the oscillation of a drop immersed in a stagnant liquid was performed in order to assure that the ALE/FE code is able to deal with calculations of surface tension in a reasonably precise way. The results showed good convergence in comparison with the analytic solution.

Although exist several experimental studies that firm the important role played by coalescing phenomena in two-phase flows, mainly around transition regimes, this issue still is challenging for MCFD methods and numerics, inasmuch as interfacial effects difficult to capture dominate the liquid thin film region. On the other hand, the introductory numerical results here obtained underpin the quality of the ALE/FE to discretize profitably the interface of an arbitrary bubble immersed in a liquid solution and boost us to pursuit deeper investigations that include LS schemes for applications enfolding bubble coalescence. In this trail, this numerical model also seeks precise concordance with experimental data and observation. Advancements and improvements in the root idea of the method so far presented are needed and the main research targets to study include: extension to threedimensional cases and modeling of the coalescence between bubbles with arbitrary surface topology, such as Taylor bubbles evolving in microchannels.

6. ACKNOWLEDGEMENTS

G.C.P.O thanks to the Science Without Borders Program/CNPq - Brazil for his scholarship granting as visitor at LTCM.

7. REFERENCES

Agrawal, K., 2013. "Bubble dynamics and interface phenomenon". *Journal of Engineering and Technology Research*, Vol. 5, No. 3, pp. 42–50.

Bloch, E.D., 1956. *A First Course in Geometric Topology and Differential Geometry*. Birkhauser.

Brackbill, J., Kothe, D.B. and Zemach, C., 1992. "A continuum method for modeling surface tension". *Journal of computational physics*, Vol. 100, No. 2, pp. 335–354.

Cheng, L., Ribatski, G. and Thome, J., 2008. "Two-phase flow patterns and flow-pattern maps: fundamentals and applications". *Applied Mechanics Reviews*, Vol. 61, No. 5, p. 050802.

Clift, R., Grace, J. and Weber, M.E., 1978. *Bubbles, Drops and Particles*. Academic Press.

Consolini, L. and Thome, J., 2010. "A heat transfer model for evaporation of coalescing bubbles in micro-channel flow". *International Journal of Heat and Fluid Flow*, Vol. 31, No. 1, pp. 115–125.

Coulibaly, A., Lin, X., Bi, J. and Christopher, D.M., 2013. "Bubble coalescence at constant wall temperatures during subcooled nucleate pool boiling". *Experimental Thermal and Fluid Science*, Vol. 44.

Donea, J., Huerta, A., Ponthot, J.P. and Rodríguez-Ferran, A., 2004. "Arbitrary lagrangian–eulerian methods". *Encyclopedia of computational mechanics*.

dos Anjos, G.R., 2012. *A 3D ALE Finite Element Method for Two-Phase Flows with Phase Change*. Ph.D. thesis, EPFL - École Polytechnique Fédéral de Lausanne, Switzerland.

Ekambara, K., Sanders, R.S., Nandakumar, K. and Masliyah, J., 2012. "Cfd modeling of gas-liquid bubbly flow in horizontal pipes: Influence of bubble coalescence and breakup". *International Journal of Chemical Engineering*, Vol. 2012.

Groß, S., Reichelt, V. and Reusken, A., 2006. "A finite element based level set method for two-phase incompressible

flows". *Computing and Visualization in Science*, Vol. 9, No. 4, pp. 239–257.

Hewitt, G.F. and Hall-Taylor, N., 1970. *Annular Two-Phase Flow*. Pergamon Press.

Jingliang, B., Xipeng, L. and Christopher, D.M., 2012. "Effects of bubble coalescence dynamics on heat flux distributions under bubbles". *AIChE Journal*.

Julia, J.E. and Hibiki, T., 2011. "Flow regime transition criteria for two-phase flow in a vertical annulus". *International Journal of Heat and Fluid Flow*, Vol. 32, No. 5, pp. 993–1004.

Li, B. and Shoppie, J., 2011. "An interface-fitted finite element level set method with application to solidification and solvation". *Communications in Computational Physics*, Vol. 10, No. 1, p. 32.

Michaelides, E.E., 2006. *Particles, Bubbles and Drops: Their Motion, Heat and Mass Transfer*. World Scientific.

Mier-Torrecilla, M.d., Idelsohn, S. and Oñate, E., 2011. "Advances in the simulation of multi-fluid flows with the particle finite element method. application to bubble dynamics". *International Journal for Numerical Methods in Fluids*, Vol. 67, No. 11, pp. 1516–1539.

Ong, C. and Thome, J., 2011. "Macro-to-microchannel transition in two-phase flow: Part 1–two-phase flow patterns and film thickness measurements". *Experimental Thermal and Fluid Science*, Vol. 35, No. 1, pp. 37–47.

Osher, S. and Fedkiw, R.P., 2001. "Level set methods: an overview and some recent results". *Journal of Computational physics*, Vol. 169, No. 2, pp. 463–502.

Quan, S., 2011. "Simulations of multiphase flows with multiple length scales using moving mesh interface tracking with adaptive meshing". *Journal of Computational Physics*, Vol. 230, No. 13, pp. 5430–5448.

Quan, S., Lou, J. and Schmidt, D.P., 2009. "Modeling merging and breakup in the moving mesh interface tracking method for multiphase flow simulations". *Journal of Computational Physics*, Vol. 228, No. 7, pp. 2660–2675.

Quan, S. and Schmidt, D.P., 2007. "A moving mesh interface tracking method for 3d incompressible two-phase flows". *Journal of Computational Physics*, Vol. 221, No. 2, pp. 761–780.

Revellin, R., Agostini, B. and Thome, J.R., 2008. "Elongated bubbles in microchannels. part ii: Experimental study and modeling of bubble collisions". *International Journal of Multiphase Flow*, Vol. 34, No. 6, pp. 602–613.

Shen, X., Hibiki, T., Ono, T., Sato, K. and Mishima, K., 2012. "One-dimensional interfacial area transport of vertical upward bubbly flow in narrow rectangular channel". *International Journal of Heat and Fluid Flow*.

Sousa, F.S.d. and Mangiavacchi, N., 2005. "A lagrangian level-set approach for the simulation of incompressible two-fluid flows". *International journal for numerical methods in fluids*, Vol. 47, No. 10-11, pp. 1393–1401.